

# ON THE REFLECTION OF SOLITONS OF THE NONLINEAR SCHRÖDINGER EQUATION

TH. KATSAOUNIS AND D. MITSOTAKIS

**ABSTRACT.** In this paper we perform a numerical study on the interesting phenomenon of soliton reflection of solid walls. We consider the 2D nonlinear Schrödinger equation as the underlying mathematical model and we use an implicit-explicit type Crank-Nicolson finite element scheme for its numerical solution. After verifying the perfect reflection of the solitons on a vertical wall, we present the imperfect reflection of a dark soliton on a diagonal wall.

## 1. INTRODUCTION

In this paper we study numerically the phenomenon of reflection of bright and dark solitons of walls. To this effect, we consider the initial and boundary value problem of a nonlinear Schrödinger (NLS) type equation

$$\begin{cases} \partial_t u - i\alpha \Delta u = i\lambda f(u) & \text{in } \Omega \times (0, T], \\ u = 0 & \text{on } \partial\Omega \times [0, T], \\ u(\cdot, 0) = u_0 & \text{in } \Omega, \end{cases} \quad (1)$$

where we assume that  $\Omega \subset \mathbb{R}^2$ , is a bounded, convex, polygonal domain,  $T < \infty$ ,  $\alpha > 0$ ,  $\lambda \in \mathbb{R}$ , and  $f(u)$  denotes the nonlinear term. In particular, we consider a nonlinear term of the form  $f(z) := |z|^{2p}z$ ,  $\frac{1}{2} \leq p \leq p^*$ , where  $p^* := 1$  denotes the critical exponent. For  $\lambda \leq 0$ , problem (1) is known as the *defocusing nonlinear Schrödinger equation*, while If  $\lambda > 0$ , problem (1) is called the *focusing nonlinear Schrödinger equation*. In this paper we will consider only the case of the cubic  $p = 1$  nonlinear Schrödinger (NLS) equation.

Models of the form (1) are widely used in many areas of applied sciences: nonlinear optics and lasers, water waves, quantum hydrodynamics and Bose-Einstein condensates, [11]. It is well known that, for  $u_0 \in H_0^1(\Omega) \cap H^2(\Omega)$  and  $\frac{1}{2} \leq p < p^*$ , (1) admits a unique solution  $u \in C([0, T]; H_0^1(\Omega) \cap H^2(\Omega)) \cap C^1([0, T]; L^2(\Omega))$ , [6]. We denote by  $\|\cdot\|$  the  $L^2$ -norm in  $\Omega$ , while for  $1 \leq q \leq \infty$ ,  $q \neq 2$ , we denote by  $\|\cdot\|_{L^q}$  the  $L^q$ -norm in  $\Omega$ . Problem (1) satisfies two conservation laws, in particular, for  $t \geq 0$ , we have

$$M(t) := \|u(t)\|^2, \quad \text{then} \quad M(t) = M(0), \quad \text{mass conservation,} \quad (2)$$

$$E(t) := \frac{1}{2} \left( \|\nabla u(t)\|^2 - \frac{\lambda}{\alpha(p+1)} \|u(t)\|_{L^{2p+2}}^{2p+2} \right), \quad \text{then} \quad E(t) = E(0), \quad \text{energy conservation.} \quad (3)$$

In this paper we focus on two aspects: a) we evaluate the Crank-Nicolson relaxation method for 2D domains discretized by completely unstructured grids and b) we study various reflections of solitons on walls for NLS type (1) of equations either focusing or defocusing.

Nonlinear Schrödinger type equations can describe waves in optical fibers, [2], as well as rogue waves in the ocean, cf. e.g. [9]. In both cases the study of the interaction of the waves with structures imposes the study of the reflection of solitons on walls. On the other hand, it is well known that in the one space dimension NLS equation (1) is an integrable system, thus one can compute analytically exact solutions describing soliton reflections. However, in two space dimensions system (1) is not integrable thus one has to rely on numerical methods for computing and studying such reflective phenomena.

The numerical method used here is based on the standard finite element method for the spatial discretization and the *relaxation Crank-Nicolson* scheme as a time marching mechanism. The relaxation Crank-Nicolson was introduced by Besse [3] and its main advantage is that evaluates the nonlinear term explicitly thus avoiding solving a costly nonlinear equation at each time step. Moreover, the relaxation scheme exhibits mass conservation, same as the standard Crank-Nicolson scheme, thus reflecting the mass conservation property of the continuous problem, cf. (2).

Due to the integrability properties of the NLS equation, the reflection of a soliton can be studied analytically only in 1D, [4, 5, 10]. In this paper after verifying the order of accuracy of the numerical

---

*Key words and phrases.* nonlinear Schrödinger equation, relaxation method, soliton reflection, dark and bright solitons.

method in space and time, we validate the efficiency of the numerical method by studying first the perfect (elastic) reflection of dark and bright solitons on vertical walls using Robin boundary conditions, [4]. Finally, we show that the reflection of a dark soliton is not perfect (inelastic) when the soliton collides on the wall at an angle.

This paper is organized as follows: in Section 2 we describe briefly the relaxation Crank-Nicolson finite element method and state its approximation properties. Section 3 contains numerical results which a) validate the numerical method and b) study the phenomenon of soliton reflection.

## 2. THE NUMERICAL METHOD

We describe briefly the numerical method used in this study. We start by presenting the relaxation Crank-Nicolson method and proceed by the fully discrete scheme. We consider a uniform partition  $t_n = nk$  of  $[0, T]$  where  $k = T/N$  and  $I_n := (t_n, t_{n+1}]$ ,  $0 \leq n \leq N-1$ , denote the fixed time step and subintervals of  $[0, T]$ , respectively. Then the standard Crank-Nicolson method for the time discretization of (1) reads as follows : we seek approximations  $U^n \in H_0^1(\Omega)$  to  $u(t_n)$ ,  $0 \leq n \leq N$ , such that

$$\begin{aligned} \bar{\partial}U^n - i\alpha\Delta U^{n+\frac{1}{2}} &= i\lambda|U^{n+\frac{1}{2}}|^{2p}U^{n+\frac{1}{2}}, \quad 0 \leq n \leq N-1, \\ \text{where } \bar{\partial}U^n &:= \frac{U^{n+1} - U^n}{k} \quad \text{and} \quad U^{n+\frac{1}{2}} := \frac{U^{n+1} + U^n}{2}, \\ U^0 &= u_0. \end{aligned} \quad (4)$$

The Crank-Nicolson relaxation method developed by Besse, [3] is based on the following equivalent form of (1):

$$\begin{cases} \phi = |u|^{2p} & \text{in } \Omega \times (0, T], \\ \partial_t u - i\alpha\Delta u = i\lambda\phi u & \text{in } \Omega \times (0, T]. \end{cases} \quad (5)$$

Motivated by (5) and (4) the relaxation method is defined by

$$\begin{cases} \frac{1}{2}(\Phi^{n+\frac{1}{2}} + \Phi^{n-\frac{1}{2}}) = |U^n|^{2p}, & 0 \leq n \leq N-1, \\ \bar{\partial}U^n - i\alpha\Delta U^{n+\frac{1}{2}} = i\lambda\Phi^{n+\frac{1}{2}}U^{n+\frac{1}{2}}, & 0 \leq n \leq N-1, \end{cases} \quad (6)$$

with  $\Phi^{-\frac{1}{2}} = |u_0|^{2p}$  and  $U^0 = u_0$ . The semidiscrete scheme (6) is of an implicit-explicit type of numerical scheme where the linear part of the differential operator is discretized implicitly, while the discretization of the nonlinear term is explicit. Such type of schemes avoid the costly solution of a nonlinear equation at each time step, as in the case of the Crank-Nicolson method (4). At the same time, the term involving the Laplacian ( $\Delta u$ ) is discretized in time implicitly, preserving good stability properties of the numerical scheme (6). Details on stability and convergence results for scheme (6) can be found in [3]. In particular, method (6) is expected to be second order accurate in time, [3]. Moreover, the relaxation scheme satisfies  $\|U^n\| = \|U^0\|$ ,  $0 \leq n \leq N$ , which is the discrete analogue of the mass conservation (2). Also, as it has been proven in [3], for  $p = 1$  and uniform time steps, the relaxation method also satisfies a discrete analogue of the energy conservation (3).

For the spatial discretization, we consider a family of conforming, shape regular triangulations  $\{\mathcal{T}\}$  of  $\Omega$ . For an element  $K \in \mathcal{T}$ , we denote its boundary by  $\partial K$  and by  $h_K$  its diameter and let  $h = \max_K h_K$ . To the triangulation  $\mathcal{T}$  we associate the finite element space  $\mathbb{V}_r$ ,

$$\mathbb{V}_r := \{\chi \in H_0^1(\Omega) : \forall K \in \mathcal{T}, \chi|_K \in \mathbb{P}^r\},$$

where  $\mathbb{P}^r$  denotes the space of polynomials in two variables of degree at most  $r$ . To introduce a fully discrete method, we will also need the definitions of the  $L^2$ -projection and of the discrete laplacian onto  $\mathbb{V}_r$ . To this end, the  $L^2$ -projection  $\mathcal{P} : L^2 \rightarrow \mathbb{V}_r$  is defined as

$$\langle \mathcal{P}v, \chi \rangle = \langle v, \chi \rangle, \quad \forall \chi \in \mathbb{V}_r,$$

and every  $v \in L^2(\Omega)$ . Moreover, the discrete laplacian  $-\Delta_h : H_0^1(\Omega) \rightarrow \mathbb{V}_r$  is defined as

$$\langle -\Delta_h v, \chi \rangle = \langle \nabla v, \nabla \chi \rangle, \quad \forall \chi \in \mathbb{V}_r, \quad (7)$$

and every  $v \in H_0^1(\Omega)$ .

We can now define the modified relaxation Crank-Nicolson-Galerkin-type fully discrete scheme. For  $0 \leq n \leq N$ , we seek approximations  $U^n \in \mathbb{V}_r$  to  $u(t_n)$  such that, for  $0 \leq n \leq N - 1$ ,

$$\begin{cases} \frac{1}{2} \left( \Phi^{n+\frac{1}{2}} + \Phi^{n-\frac{1}{2}} \right) = \mathcal{P} (|U^n|^{2p}), \\ \frac{U^{n+1} - U^n}{k} - i\alpha \Delta_h U^{n+\frac{1}{2}} = i\lambda \mathcal{P} \left( \Phi^{n+\frac{1}{2}} U^{n+\frac{1}{2}} \right), \end{cases} \quad (8)$$

with  $\Phi^{-\frac{1}{2}} = \mathcal{P} (|u_0|^{2p})$ ,  $U^0 = \mathcal{P} u_0$ . Formally we expect the method to be of second order accurate in time and of  $r + 1$ -order accurate in space, which can be expressed by an error estimate of the following form

$$\max_{0 \leq n \leq N} \|U^n - u(t_n)\| \leq C (h^{r+1} + k^2), \quad (9)$$

where  $C$  is a constant depending on the exact solution  $u$  of (1) and data of the problem, but it is independent of  $h$  and  $k$ .

At each time step  $t_n$ , given an approximation  $U^n \in \mathbb{V}_r$  and  $\Phi^{n-\frac{1}{2}}$ , the algorithm proceeds first by computing the new value  $\Phi^{n+\frac{1}{2}}$ . The computational cost of this update is relatively low since it involves only the cost of the projection of the right hand side in the first relation of (8). The cost of such projection amounts to the solution of a real linear system with the mass matrix and real right hand side since  $\Phi^{n+\frac{1}{2}}$  is real valued. The second part of the algorithm (8), involves the update of the right hand side via a projection and the solution of a complex-valued linear system. The system matrix of this linear system, does not change in time, thus can be computed and factored only once in the initial step of the algorithm. An alternative approach for solving the linear systems is by using an appropriate conjugate gradient type method, since the system matrices in both steps are positive definite. Therefore the algorithmic complexity of method (8) at each time step is at most of  $O(m^2)$  where  $m$  denotes the size of the matrix, thus making the method computationally very attractive.

### 3. NUMERICAL EXPERIMENTS

In this section we first validate numerically the method (8) by means of verifying the convergence rates in space and time of the error estimate (9). Furthermore, we present some results concerning the head on or oblique soliton reflection of solid walls.

**3.1. Method validation.** To validate the method numerically we perform a series of numerical experiments verifying the correct order of convergence as presented by the *a priori* error estimate (9). To facilitate the process and be able to compute the exact error between the true and approximate solution, we choose to work with a solution of a non-homogeneous version of equation (1) and in particular we choose

$$u(x, y, t) = e^t x(1 - x)y(0.5 - y), \quad (10)$$

which is an exact solution of (1) with appropriate right-hand side, and  $p = 1$ ,  $\alpha = 1$ ,  $\lambda = -2$ , zero Dirichlet boundary conditions, and  $u_0(x, y) = u(x, t, 0)$ . For the computation of the errors in time we use quadratic finite elements ( $r = 2$ ) in space, the computational domain is the rectangle  $\Omega = [0, 1] \times [0, 0.5]$  and final time  $T = 4$ . The domain is covered by an unstructured in general triangulation  $\mathcal{T}$  of good quality (with triangle minimum angle not to be less than  $31^\circ$ ). To verify the error convergence rates we compute the *experimental order of convergence* (EOC). Let  $\ell \in \mathbb{N}$  counts the different realizations (runs) and let  $h_\ell$ ,  $k_\ell$ ,  $\mathcal{E}_\ell$  be the spatial mesh size, time step and error respectively. Choosing a very small spatial mesh size (in our experiments we used 192802 triangles) the corresponding spatial component of the error is negligible and the temporal EOC is computed as  $\text{EOC} = \frac{\log(\mathcal{E}_{\ell+1}/\mathcal{E}_\ell)}{\log(k_{\ell+1}/k_\ell)}$ . The temporal EOC is found to be 2 and is presented Table 1.

$\ell$	1	2	3	4	5
$k_\ell$	0.5	0.25	0.08	0.0625	0.03125
$E_\ell$	$9.02 \times 10^{-3}$	$2.27 \times 10^{-3}$	$2.35 \times 10^{-4}$	$1.43 \times 10^{-4}$	$3.49 \times 10^{-5}$
EOC	—	1.9880	1.9905	2.0020	2.0412

TABLE 1. Temporal numerical errors and experimental orders of convergence

The spatial errors can be computed in a similar manner. Specifically, in order to estimate the spatial convergence rates we take the domain to be  $\Omega = [0, 2] \times [0, 2]$  and exact solution  $u(x, y, t) = e^t(1 - \cos(2\pi x))\sin(2\pi y)$  along with the appropriate non-homogeneous term. Now we take  $T = 0.1$  and  $k = 2 \cdot 10^{-5}$ , thus the temporal component of the error is negligible. The triangulation now is structured and consisted of equal right-angle triangles with perpendicular sides of length  $h = \sqrt{2/N}$ , where  $N$  is the number of triangles. The number of triangles we tested were  $N = 32, 128, 512, 2048, 8192, 32768$ . The numerical experiments confirmed the expected orders of convergence. The numerical results are depicted in Figure 1, where the results are presented in logarithmic scales.

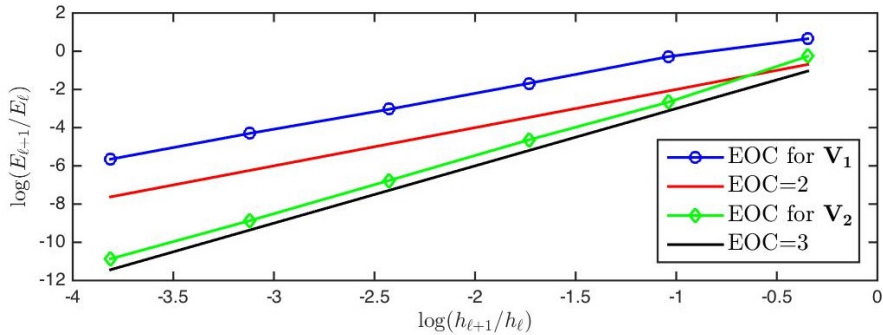


FIGURE 1. Experimental orders of convergence for linear and quadratic elements.

**3.2. Perfect Reflection of Solitons.** The focusing NLS equation ( $p = 1$ ,  $\lambda = 2$ ) has bright soliton solutions of the form  $u_b(x, y, t) = \eta \operatorname{sech}[\eta(x + 2\xi t)] e^{-i\theta}$  where  $\theta = \xi x + (\xi^2 - \eta^2)t$ , while the defocusing NLS equation ( $p = 1$ ,  $\lambda = -2$ ) admits dark soliton solutions of the form  $u_d(x, y, t) = \eta [\cos \xi + i \sin \xi \tanh(\sin \xi \eta(-x + 2\eta \cos \xi t))] e^{-2i\eta^2 t}$ , cf. e.g. [1]. The parameters  $\xi$  and  $\eta$  are chosen appropriately.

In this section we verify that the reflection of a soliton of the NLS equation is *perfect* when the soliton collides with a vertical wall at zero angle. The reflection is called *perfect* if the reflected wave has the same shape as the original soliton but different direction of propagation. This behaviour has been studied analytically in [4, 5, 10] for the integrable NLS equation in one space dimension. We tested the reflection of a bright soliton for the focusing NLS equation with  $\lambda = 2$ ,  $\eta = 2$ ,  $\xi = 2$  and zero Neumann boundary conditions in the domain  $\Omega = [-5, 5] \times [-1, 1]$ , while quadratic elements were used. The results of the perfect reflection are presented in Figure 2, depicting the amplitude of the wave. It is known that the solitons of the NLS equation suffer by an instability of focusing type. In order to ensure that the propagation of the soliton remains stable during the simulation we took 74496 triangles ensuring a very fine spatial grid and a small time-step  $k = 5 \times 10^{-3}$ . During the experiment the mass  $M$  was conserved with value 7.999999 while the energy  $E$  was conserved to 10.5 up to  $T = 3$ .

Similarly, the perfect reflection of the dark soliton of the defocusing NLS equation with  $\lambda = -2$ ,  $\eta = 1$ ,  $\xi = \pi/4$  and with zero Neumann boundary conditions are presented in Figure 3, showing the amplitude of the wave. Since the dark solitons are in general stable waves we used coarser grids than the previous experiment. Specifically, we used an unstructured mesh consisted of 18624 triangles and time-step  $k = 5 \times 10^{-2}$ . Due to the stability properties of the defocusing NLS equation, the mass  $M$  was conserved with more digits than in the case of the focusing NLS equation with value 17.1763733098 while the energy  $E$  was conserved to 8.119 up to  $T = 15$ . It is noted that other boundary conditions such as zero Dirichlet on the left and right boundaries will result to a perfect reflection as well but the interaction of the soliton with the boundary is different. For the differences between the two reflections we refer to [4, 5].

**3.3. Reflection of a dark soliton on a diagonal wall.** The reflection of the dark soliton on a vertical wall presented in the previous section was perfect in the sense that the reflected wave had the same shape

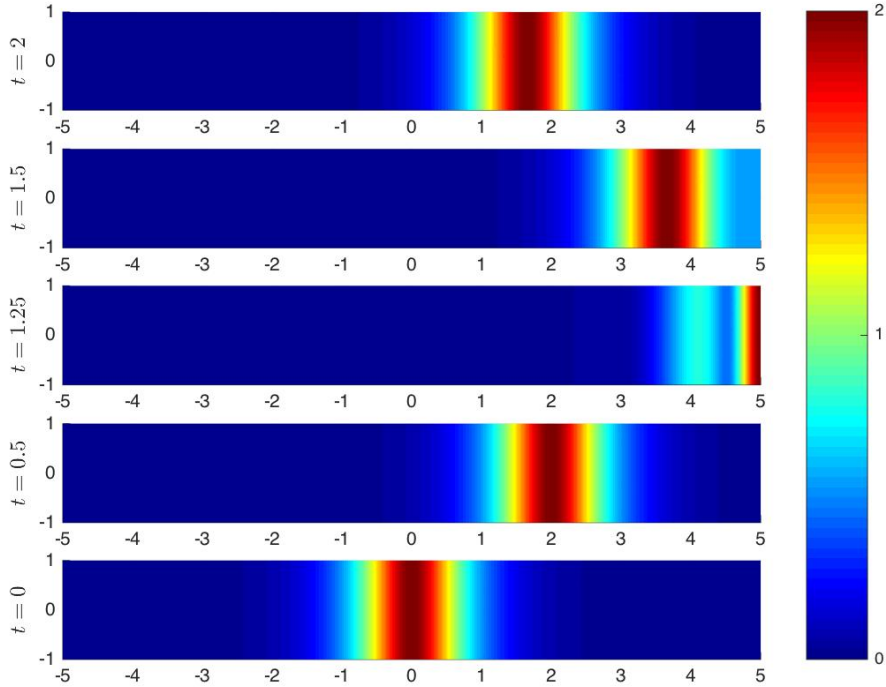


FIGURE 2. Perfect reflection of a bright soliton.

with the original soliton. We close this paper with the study of the reflection of the same dark soliton of the defocusing NLS on a diagonal wall. Since the NLS equation in a two-dimensional domain is not integrable there is no analytical solution describing such a complicated reflection. The domain that we used here is a trapezoidal domain with vertices  $(-8, -1)$ ,  $(-7, 1)$ ,  $(8, 1)$  and  $(8, -1)$  while the triangular grid consisted of 28592 triangles. In this experiment we use also quadratic finite elements. The reflection is not perfect and is presented in Figure 4, depicting the amplitude of the wave. As the wave approaches the left side of the boundary, diffraction of the incident wave is being observed. The diffraction of the wave causes the distortion of the soliton while the reflected wave has an oscillatory structure in front and behind of the main pulse. Although it is known that dark solitons exhibit a transverse instability to perturbations with sufficiently long wavelength, [7, 8], the reflected wave remained stable and no collapse or any other blow-up phenomenon was observed up to time  $T = 15$ . During this experiment the mass  $M$  retained the value (conserving the digits shown) 28.1716833830 and the energy  $E$  was conserved to 13.61 up to  $T = 15$ . Analogous observations can be made in the case of the focusing NLS equation and are not presented here.

#### ACKNOWLEDGMENTS

Dimitrios Mitsotakis would like thank Profs G. Biondini, S. Flach and B. Ilan for valuable discussions on the properties of the NLS equation. This work was supported by the Victoria University of Wellington Research Establishment Grant (Grand ID 208964).

#### REFERENCES

- [1] M. Ablowitz, *Nonlinear Dispersive Waves: Asymptotic Analysis and Solitons*, Cambridge Texts in Applied Mathematics, 2011.
- [2] G. Argawal, *Nonlinear Fiber Optics*, Academic Press, San Diego, 1989.
- [3] Ch. Besse, *A relaxation scheme for the nonlinear Schrödinger equation*, SIAM J. Numer. Anal. **42** (2004) 934–952.
- [4] G. Biondini, G. Hwang, *Solitons, boundary value problems and a nonlinear method of images*, J. Phys. A: Math. Theor. **42** (2009), 205207.
- [5] G. Biondini, A. Bui, *On the nonlinear Schrödinger equation on the half line with homogeneous Robin boundary conditions*, Stud. Appl. Math. **129** (2012), 249–271.
- [6] H. Brezis, T. Gallouet, *Nonlinear Schrödinger evolution equations*, Nonlinear Anal. **4** (1980), 677–681.

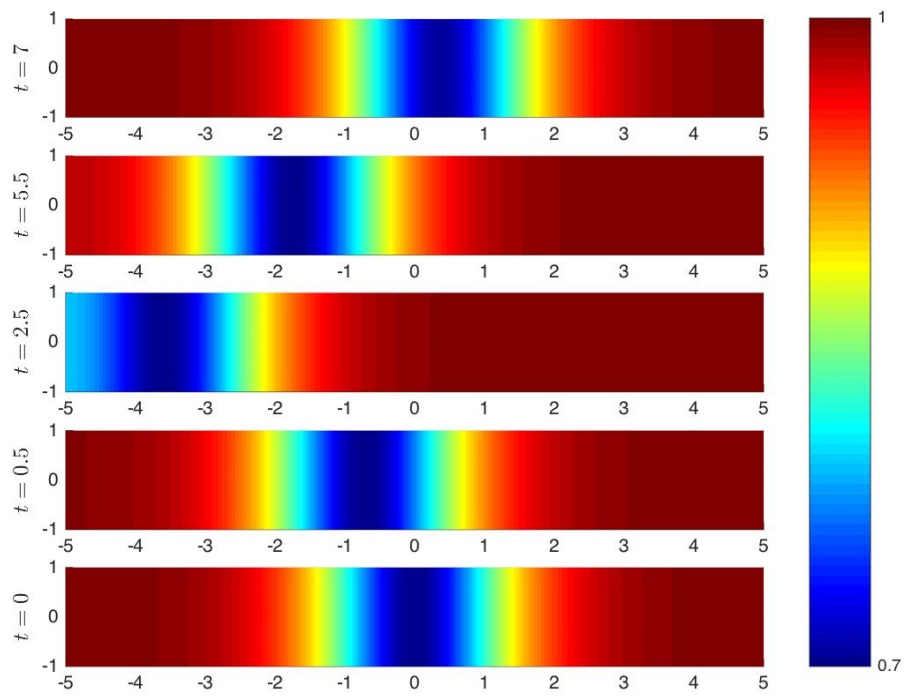


FIGURE 3. Perfect reflection of a dark soliton.

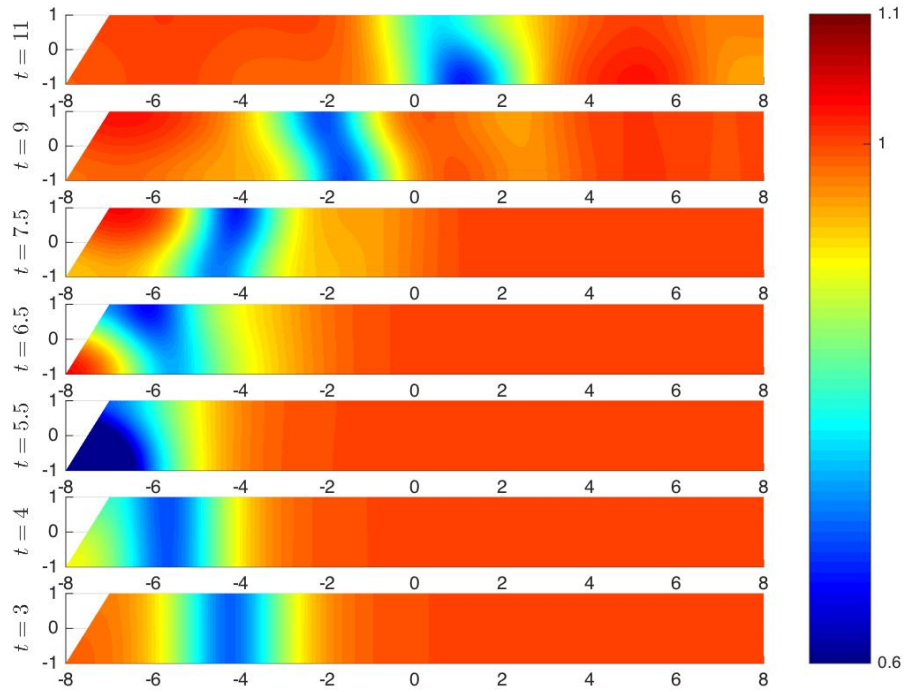


FIGURE 4. Reflection of a dark soliton by a diagonal wall.

- [7] E.A. Kuznetsov, S.K. Tyrityn, *Instability and collapse of solitons in media with a defocusing nonlinearity*, Sov. Phys. JETP **67** (1988), 1583–1586.
- [8] M. Hoefer, B. Ilan, *Dark solitons, dispersive shock waves, and transverse instabilities*, Multiscale Model. Simul. **10** (2012), 306–341.
- [9] A.R. Osborne, M. Onorato, M. Serio, *The nonlinear dynamics of rogue waves and holes in deep-water gravity wave trains*, Physics Letters A **275** (2000), 386–393.
- [10] V. O. Tarasov, *The integrable initial-boundary value problem on a semiline: nonlinear Schrödinger equation and sine-Gordons*, Inv. Prob. **7** (1991), 435–449.
- [11] C. Sulem, P.-L. Sulem, *The nonlinear Schrödinger equation: self-focusing and wave collapse*, vol. 139, Springer, 1999.

(Theodoros Katsaounis) KING ABDULLAH UNIVERSITY OF SCIENCE AND TECHNOLOGY (KAUST), COMPUTER, ELECTRICAL, MATHEMATICAL SCIENCE AND ENGINEERING (CEMSE), THUWAL 23955-6900, KINGDOM OF SAUDI ARABIA, & IACM-FORTH, HERAKLION, GREECE

*E-mail address:* theodoros.katsaounis@kaust.edu.sa

(Dimitrios Mitsotakis) VICTORIA UNIVERSITY OF WELLINGTON, SCHOOL OF MATHEMATICS, STATISTICS AND OP. RESEARCH,, PO Box 600, WELLINGTON 6140, NEW ZEALAND

*E-mail address:* dimitrios.mitsotakis@vuw.ac.nz